High-Accuracy Algorithms for Computational Aeroacoustics

David P. Lockard*
George Washington University, Hampton, Virginia 23681-0001
and
Kenneth S. Brentner[†] and H. L. Atkins[‡]
NASA Langley Research Center, Hampton, Virginia 23681-0001

This paper presents an analysis of high-bandwidth operators developed for use with an essentially nonoscillatory (ENO) method. The spatial operators of a sixth-order ENO code are modified to resolve waves with as few as 7 points per wavelength (PPW) by decreasing the formal order of the algorithm. Numerical and analytical solutions are compared for the model problems of plane-wave propagation and sound generation by an oscillating sphere. These problems involve linear propagation, wave steepening, and shock formation. An analysis of the PPW required for sufficient accuracy shows that low-order algorithms need an excessive number of grid points to produce acceptable solutions. In contrast, high-order codes provide good predictions on relatively coarse grids. The high-bandwidth operators produce only modest improvements over the original sixth-order operators for nonlinear problems in which wave steepening is significant; however, they clearly outperform the original operators for long-distance linear propagation. Because the high-bandwidth operators have the same stencil as the original sixth-order operators, these gains are achieved with no additional computational work.

Introduction

ACOUSTICS is often thought to deal with only linear phenomena; however, in aeroacoustics an equal interest exists in the sound-generation mechanisms and the effect of large mean flow variations (including shocks) on acoustic propagation. Acoustic signals are often many orders of magnitude smaller than the flowfield variations that generate the sound. Damping and dispersion of propagating waves are not desirable and must be minimized.

Several possible approaches are available for obtaining high accuracy with current computational fluid dynamics (CFD) (finite difference) types of codes. One straightforward method for obtaining high accuracy is to use a very fine grid with a standard low-order method. Although this method is possible in principle, such calculations are not truly feasible because of the enormous computer memory and time requirements. Another approach, illustrated by the recent work of Thomas and Roe,[1] is to increase the accuracy by incorporating more of the flow physics into the algorithm design. Although preliminary results for one-dimensional problems are extremely good, general multidimensional formulations are still under development. Alternatively, the accuracy can be improved by increasing the stencil size and thereby providing more information for the scheme at any grid point. Despite some drawbacks, increased stencil size appears to be one of the most practical means of obtaining the accuracy required for aeroacoustic computations and will be the main subject of this paper.

Algorithms that use such stencils are most commonly designed to achieve a maximum order property for a given stencil width. An alternative, pursued by Lele[2] is to consider both order property and bandwidth characteristics in the design of the scheme. In this approach, the order of the operator is selected to be less than the maximum possible for the stencil width, and the additional degrees

of freedom are used to improve the bandwidth characteristics of the method. Lele used the additional degrees to maximize the wave number for which all longer waves were resolved within a specified criterion. Tam chose to minimize an integral of the error over a portion of the spectrum. Both Lele and Tam et al. restricted their optimizations to central-difference algorithms so that amplitude error would be inherently minimal. However, this restriction leads to stability problems that must be dealt with through the use of filters or explicit dissipation terms. The aforementioned researchers have been moderately successful in applying these filters and dissipation terms; however, the optimal filter sometimes varies depending on whether or not shocks are present and whether the shocks are resolved or captured.

In his thesis, Lockard[4] recognized that deficiencies in the algorithms of both Lele and Tam arose because both methods attempted to resolve wavelengths shorter than the stencil, which resulted in relatively large deviations from the differential operator over an important part of spectrum. In the work of Lockard, the optimization approach of Tam et al. was modified to focus on the portion of the spectrum that was resolved with 7 or more points per wavelength (PPW). Recently Tam and Shen[5] made the same observation and designed an improved operator that was optimized to resolve $2\pi/1.1$ (≈ 5.7) or more PPW.

In this paper, we present an analysis of the optimized operators derived in Ref. 4. However, we begin with several numerical examples to illustrate the deficiencies of traditional low-order methods and the potential improvements to be gained through the use of more accurate methods. Although similar illustrations can be found elsewhere, the importance of this point merits reiteration. We also introduce a metric, derived from Fourier analysis, which is helpful in assessing the PPW requirements of a particular scheme.

In the second portion of this work, we review the optimization procedure of Tam and his colleagues and its modification to treat upwind operators. The modified optimization procedure is used to derive a complete set of stencils needed by an existing sixth-order essentially nonoscillatory (ENO) shock-capturing method. We follow up with numerical examples of the modified ENO scheme for one- and two-dimensional model problems for which analytical solutions exist. Further detail in regard to the new high-bandwidth operators and more numerical examples of their use can be found in Ref. 4.

*Graduate Student, Joint Institute for Advancement of Flight Sciences; currently at Pennsylvania State University, University Park, PA 16802.
†Research Engineer, Aerodynamic and Acoustic Methods Branch, Fluid Mechanics and Acoustics Division. Senior Member AIAA.
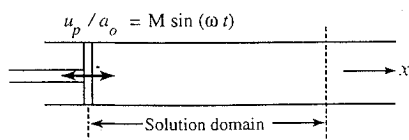‡Research Scientist, Aerodynamic and Acoustic Methods Branch, Fluid Mechanics and Acoustics Division. Member AIAA.

Numerical Example

For instructional purposes, we first demonstrate the poor results typical of low-order methods when applied to the propagation of

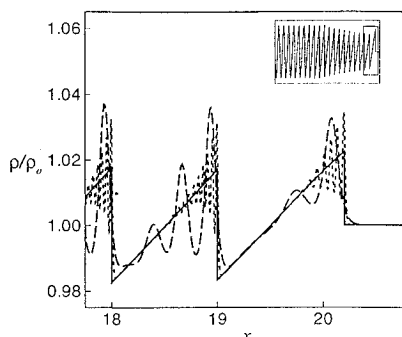Fig. 1 Schematic representation of plane-wave problem.

Fig. 2 Low-order plane-wave solution for M = 0.025 and ω = 2π after initial wave front has traveled 20 wavelengths (ν = 0.5, k_2 = 0.3, and k_4 = 1/32): ————, Whitham's solution; — — —, 91 PPW; and - - - - -; 463 PPW.
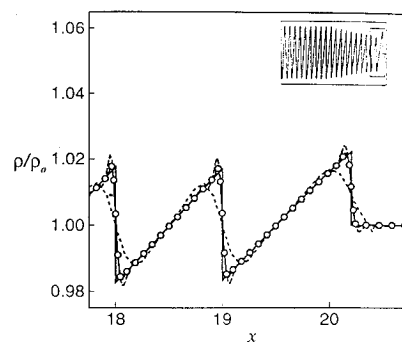

Fig. 3 High-order plane-wave solution for M = 0.025 and ω = 2π after initial wave front has traveled 20 wavelengths (ν = 0.5): ————, Whitham's solution; — — — —, fourth-order central-difference (k_2 = 0.3 and k_4 = 1/32), 64 PPW; - - - - -, sixth-order ENO, 12 PPW; and —— o———, sixth-order ENO, 50 PPW.

acoustic waves over a significant distance. The problem of one-dimensional plane-wave propagation is an appropriate model problem to test a typical low-order algorithm. This problem, shown schematically in Fig. 1, consists of a piston that begins to oscillate sinusoidally to form a wave train, which propagates down a duct into an initially undisturbed, inviscid medium. This problem is particularly useful because the initial waves propagate essentially in a linear manner but gradually steepen and eventually form shocks, which tend to fill the spectrum. For low-amplitude waves, Whitham[6] has developed an analytical solution that incorporates shock fitting, which is suitable for direct comparison with numerical solutions. Furthermore, because the problem is one dimensional, the solution can be numerically computed for long propagation distances and for high PPW.

For our example, the one-dimensional Euler equations

$$\frac{\partial \mathbf{U}}{\partial t} + \nabla \cdot \mathbf{F} = 0 \qquad (1)$$

with

$$\mathbf{U} = \begin{Bmatrix} \rho \\ \rho u \\ \rho E \end{Bmatrix}, \qquad \mathbf{F} = \mathbf{U}u + \begin{Bmatrix} 0 \\ p \\ pu \end{Bmatrix}$$

are solved numerically with a cell-centered second-order finite volume method that uses the classical four-stage fourth-order Runge-Kutta algorithm for time integration. An adaptive combination of second and fourth differences by Jameson et al.,[7] with coefficients denoted k_2 and k_4, is utilized for the required artificial dissipation. This scheme is representative of a typical central-difference low-order algorithm. The problem was modeled numerically by moving the grid at the speed of the piston and applying the no-penetration condition on the piston face. Additional dependent variables needed at the piston were obtained by third-order extrapolation from the interior. The calculation was stopped before the wave encountered the boundary at the other end of the duct, so that reflections were not produced.

A solution from the low-order code is compared with Whitham's[6] solution in Fig. 2. The initial wave front has traveled approximately 20 wavelengths. The solution computed with 91 PPW oscillates around the analytical solution, but the shock position actually agrees well. When 463 PPW are used in the computation, the numerical result is better; however, a high-frequency oscillation exists near the shock. The prediction might have been expected to be highly damped because of the adaptive first-order dissipation that is activated near shocks, but this was not observed. An increase in the dissipation coefficients suppresses the oscillations by eliminating

the higher modes; however, this cannot be done without also causing a significant artificial decay as the wave propagates. Clearly, a more accurate solution is needed even though an impractically large number of PPW were used.

High-order methods offer one avenue for achieving greater accuracy. Higher order truncation errors can be achieved through the use of larger stencils, which in effect give the discrete operator more information. The computational work increases on a per-point basis with high-order algorithms, and additional problems can occur with boundary conditions and grid metrics. Nevertheless, high-order algorithms usually produce much better solutions than their low-order counterparts.

To demonstrate the improvement in using high-order algorithms, two high-order codes were utilized on the plane-wave problem. The first code was developed by replacing the second-order spatial operator in the low-order code with a fourth-order central-difference operator. The artificial-dissipation operator was unchanged. The second and primary high-order code utilized in this work was developed by Atkins.[8] In Atkins' code, the conservation form of the Navier–Stokes equations is applied at each grid point in a domain of interest. The code was exercised in an Euler mode for this work. The spatial derivatives are approximated at an order of truncation error specified as part of the input. The code operates in one, two, and three dimensions and has been modified to solve axisymmetric problems.[4]

A unique feature of Atkins' code is the inclusion of ENO methodology. The ENO method is able to capture shock waves and remain formally high order in smooth regions of the flow through a stencil-shifting capability. Hence, a complete set of stencils from fully left to fully right shifted are available to represent the derivative. The algorithm that chooses the stencil is designed to select a preferred stencil whenever the solution is smooth. The preferred stencil in this code is one that is biased upwind by one-half cell. A flux-splitting technique ensures that all waves are properly upwinded and that no additional (explicit) dissipation is needed. Time integration is performed with a third-order Runge-Kutta algorithm developed by Shu.[9] A more detailed description of Atkins' code can be found in Ref. 8.

Figure 3 illustrates the dramatic improvement obtained when the second-order derivative operator is replaced with a higher order operator. None of the high-frequency oscillations associated with the standard low-order algorithm are evident in these results. The fourth-order central-difference result has a slight overshoot on each side of the shock but otherwise follows the analytical solution very well. The sixth-order ENO computation gives a reasonable solution even when only 12 PPW were used in the computation. The lack of sharpness is because the number of PPW is small; the particular ENO code used here is known to distribute a shock over approximately four points. When 50 PPW were used, it was nearly indistinguishable from the analytical solution.

Assessing Accuracy Requirements

The plane-wave problem demonstrates that a significant improvement can be obtained by using high-order codes, but it is difficult to judge a priori what grid resolution will be necessary both to resolve the waves adequately and to ensure that the numerical error

is sufficiently small. Some measure of the PPW required for a particular level of allowable error would be useful both in defining the computational grid and in comparing different numerical schemes.

A Fourier analysis of the advection equation gives an initial indication of the damping and dispersion errors associated with a numerical wave-propagation algorithm. This analysis yields the amplification factor G and the phase ϕ of the discrete numerical scheme as a function of the Courant-Friedrichs-Lewy (CFL) number ν and the parameter $\beta = 2\pi/\text{PPW}$. A graph of the PPW vs wavelengths traveled would be a practical assessment tool. The following implicit equations in β can be used to make such graphs. Both the amplitude and phase error must be considered. If n is the number of wavelengths traveled and ϕ_e is the phase of the exact solution, then a measure of the deviation of the numerical solution from the exact value can be defined as

$$\text{amplitude error} = \left|1 - |G(\nu, \beta)|^{\frac{2\pi n}{\nu\beta}}\right| \leq 10\% \qquad (2)$$

and

$$\text{phase error} = \frac{2\pi n}{\nu\beta}|\phi(\nu, \beta) - \phi_e| \leq 10\% \qquad (3)$$

Equation (3) ensures that the solution will not deviate from its correct value by more than 10% due to phase error; hence it is a more quantitative measure of error than phase speed and can be directly compared with the amplitude error. In this paper, 10% is arbitrarily chosen as the maximum allowable error for the definitions in Eqs. (2) and (3). When multiple values of β satisfy this criterion, the value that corresponds to the highest PPW requirement (or the lowest β) is selected to ensure that all longer waves (or the same wave on a finer grid) will also meet the criterion. Fourier analysis, and hence the error measure defined in Eqs. (2) and (3), is exact for linear problems, but it has been found to be a useful predictive measure even for nonlinear work.

As an example of the use of this metric, Fig. 4 shows the minimum PPW necessary to keep the error within the allowable range as a function of wavelengths traveled for the second-order central-difference code used in the previous section. For this analysis, the third-order dissipation coefficient was set to $1/32$, and the first-order dissipation was neglected. Notice in the figure that the PPW required to satisfy the phase constraint is considerably higher than that required to satisfy the amplitude constraint; hence, phase error dominates this algorithm. Figure 4 suggests that 91 PPW are necessary to propagate the wave 20 wavelengths; hence, the motivation for selecting this resolution in Fig. 2.

Because an arbitrary wave is considered to be a summation of sinusoidal components in Fourier analysis, the individual components must clearly be resolved to some acceptable degree. The most stringent requirement placed on the flow solver results from the application of the error criterion [Eqs. (2) and (3)] to the highest harmonic in the flow. For the case in Fig. 2, it is estimated that 463 PPW are required to resolve the third harmonic. (The third harmonic travels 60 wavelengths; hence, 154.3 PPW are required for the third harmonic, and $3 \times 154.3 = 463$ points per fundamental wavelength.)

The PPW requirements for the fourth-order central-difference operator and sixth-order preferred stencil of the ENO operator are
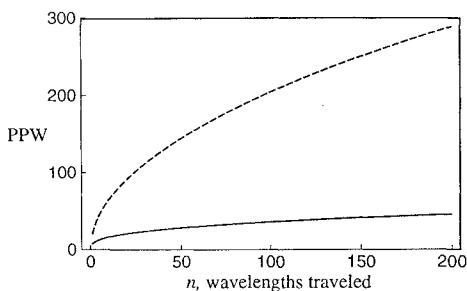

Fig. 4 PPW requirements based on advection equation for second-order central-difference code with $\nu = 0.5$ and $k_4 = 1/32$: ———, amplitude requirement, and - - - - -, phase requirement.
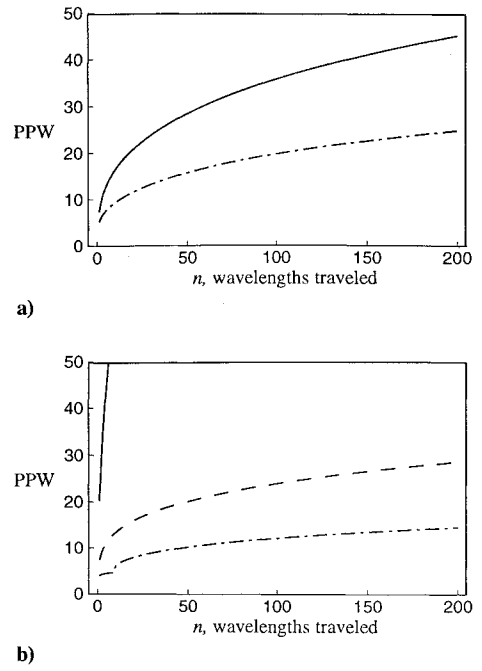

a)

b)

Fig. 5 Comparison of PPW requirements based on advection equation of high- and low-order schemes for $\nu = 0.5$: ———, second-order central-difference; — — —, fourth-order central-difference; and — - —, sixth-order preferred ENO; a) amplitude requirement and b) phase requirement.

compared in Fig. 5 with the second-order central-difference operator. The amplitude error is the same for both central-difference algorithms because they use identical dissipation terms. Notice, however, that the amplitude error dominates the phase error for both of the high-order methods. This explains the lack of oscillations and the slight damping of the solution. In Fig. 3, the 64-PPW case was chosen to resolve the third harmonic with the fourth-order central-difference code; 12 and 50 PPW resolve the first and third harmonics, respectively, for the sixth-order preferred stencil used in the ENO calculations. The sample computations demonstrate that the PPW plots provide a good a priori indication of the performance of the numerical methods. This conclusion has also been supported quantitatively in Ref. 4.

High-Bandwidth Algorithms

The bandwidth of a discrete operator refers to the range of wave numbers resolved by the operator. One strategy to create operators that are useful over a larger bandwidth is to reduce the order property below the maximum order possible for a given stencil. The reduced order provides additional degrees of freedom that can be used to optimize the operator. The stencil and, thus, the computational effort remain identical to the original operator.

The discrete approximation to the derivative operator may be written in the form

$$\frac{\partial f}{\partial x}(x) \approx \frac{1}{\Delta x}\sum_{j=-\mathcal{M}}^{\mathcal{N}} a_j f(x + j\Delta x) \qquad (4)$$

where a_j are unknown coefficients and $\mathcal{M}$ and $\mathcal{N}$ identify the discrete points utilized by the operator. The right-hand side of Eq. (4) can be expanded in a Taylor series to determine the relations between the coefficients that produce a desired order of truncation error $\mathcal{R}$. If $\mathcal{R} < \mathcal{M} + \mathcal{N}$, then the Taylor relations do not uniquely determine all of the coefficients, and the number of degrees of freedom available for optimization is $\mathcal{M} + \mathcal{N} - \mathcal{R}$.

The application of a Fourier transform to Eq. (4) gives

$$ik\mathcal{F}(k) \approx \left(\frac{1}{\Delta x}\sum_{j=-\mathcal{M}}^{\mathcal{N}} a_j e^{ijk\Delta x}\right)\mathcal{F}(k) \qquad (5)$$

where $\mathcal{F}(k)$ is the transform of $f(x)$ and k is the transform variable. We can then define β', which is the discrete approximation to the exact normalized wave number $\beta \equiv k\Delta x$, as

$$\beta' \equiv -i \sum_{j=-\mathcal{M}}^{\mathcal{N}} a_j e^{ij\beta} \tag{6}$$

The error of the numerical operator for a given wave number is simply $\epsilon_\beta \equiv |\beta' - \beta|$.

Lele's optimization strategy was to maximize the wave number β_f for which ϵ_β was less than a specified criterion for all $\beta \leq \beta_f$. Because Lele's work was with compact operators, the basic form of his derivative operator was different from that of Eq. (4). Tam's approach was to minimize the objective function

$$\mathcal{I} \equiv \int_{-\beta_0}^{\beta_0} \epsilon_\beta^2 \, d(\beta) \tag{7}$$

where β_0 prescribes the range of the normalized wave number spectrum for which the optimization is performed. The relation between β and PPW is $\beta = 2\pi/\text{PPW}$. Tam et al.[3] and Tam and Webb,[10] in their earlier work, optimized the operators with $\beta_0 = \pi/2$, which corresponds to 4 PPW. In later work,[5] β_0 was reduced to 1.1, which corresponds to approximately 5.7 PPW.

High-Bandwidth ENO Methods

The ENO methodology avoids oscillations by allowing the flux stencil to shift away from discontinuities. In the ENO code utilized here, the process of choosing the stencil has been separated from the process of evaluating the flux. High-bandwidth operators are easily implemented by providing the code with a new set of coefficients for all possible flux stencils (fully left shifted to fully right shifted). The actual ENO code requires flux operators; however, we present the results in terms of the associated derivative operators.

Because these operators are, in general, not central-difference operators, the objective function is modified to allow more control over the real and imaginary parts of the error. The modified objective function is

$$\mathcal{I} \equiv \int_{-\beta_0}^{\beta_0} \{\sigma[\text{Re}(\beta' - \beta)]^2$$

$$+ (1-\sigma)[\text{Im}(\beta') - \gamma \sin^\mu(\beta/2)]^2\} d(\beta) \tag{8}$$

The σ term is a weighting function that allows emphasis to be placed on either the real or the imaginary part. Tam et al.[3] used a similar weighting in the context of temporal operators. The sine term allows some control over the stability and high-frequency damping by biasing the imaginary part in a favorable direction. The parameter γ should always be less than or equal to 0, and μ is a positive integer. The complete set of optimized high-bandwidth seven-point derivative operators can be found in Ref. 4. Most of the operators were derived using the following parameters: $\mathcal{R} = 3$ (formally third order), $\beta_0 = 2\pi/7$, $\gamma = -13/32$, $\sigma = 1/5$, and $\mu = 8$. However, γ was set to 0 for the central-difference operator ($\mathcal{M} = \mathcal{N} = 3$), and the formal order property of the fully left-shifted operator was reduced to 2 ($\mathcal{R} = 2$ for the $\mathcal{M} = 6$ and $\mathcal{N} = 0$ case).

The algorithm for choosing the stencil within the ENO code is designed to pick a predetermined preferred stencil whenever the solution is smooth. The preferred sixth-order operator used in the original code was constructed from an average of the sixth-order upwind operator ($\mathcal{M} = 4$ and $\mathcal{N} = 2$) and the sixth-order central-difference operator ($\mathcal{M} = \mathcal{N} = 3$). The coefficients of the high-bandwidth preferred operator that result from averaging the optimized central and upwind operators are

$$\begin{aligned}
a_{-4} &= 0.01039302092790538 \\
a_{-3} &= -0.08469749427253499 \\
a_{-2} &= 0.34203118305695955 \\
a_{-1} &= -1.05268128383328493 \\
a_0 &= 0.28727412440422240 \\
a_1 &= 0.58616247381945879 \\
a_2 &= -0.09814428166337050 \\
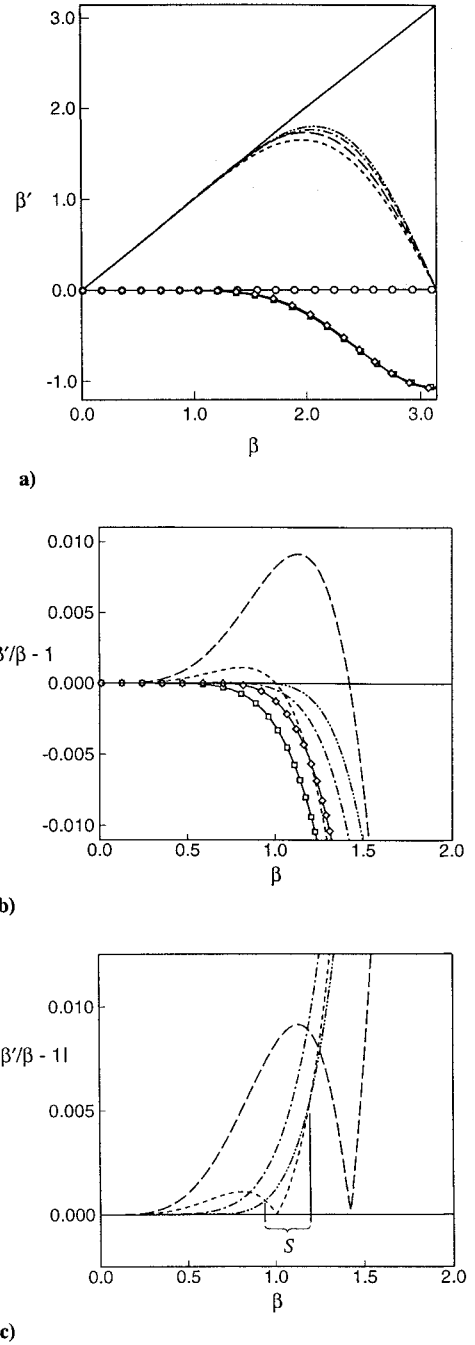a_3 &= 0.00966225756064431
\end{aligned}$$

a)

b)

c)

Fig. 6 Comparisons of standard and high-bandwidth preferred ENO operators with high-bandwidth operators taken from Refs. 3 and 5: (——— and ——o———) (Re and Im), exact solution; — — —, Tam-1; - - - -, Tam-2; (——— — — and ——□———) (Re and Im), standard sixth order; and (— - - — and ——◇———) (Re and Im), third-order high bandwidth.

Fourier analysis of the high-bandwidth preferred ENO operator is shown in Fig. 6 along with that of the original preferred ENO operator and two operators taken from Refs. 3 and 5 (denoted Tam-1 and Tam-2, respectively). In Fig. 6a, which presents the results in the form most commonly seen in literature, the results are difficult to distinguish from the exact curve for $\beta < 1$. Figure 6b, which shows the difference between the discrete and exact solutions, allows this region to be examined more closely. The difficulty in resolving small wavelengths becomes apparent. Although Tam's operators briefly pass through the exact solution at relatively large values of β, the deviation from the correct result for smaller values is excessive. If the region of optimization is decreased from $\beta_0 = \pi/2$ to $\beta_0 = 1.1$ (as Tam and his colleagues have done in going from Tam-1 to Tam-2), then a marked improvement occurs; however, a noticeable overshoot
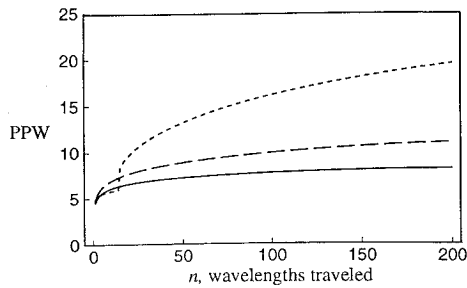
Fig. 7   Comparison of PPW requirements for three spatial operators:
———, third-order high bandwidth; — — —, standard sixth order; and
- - - - -, Tam-2.

Fig. 8   Convergence comparison for advection equation of preferred spatial operators for ENO code: ---□---, standard sixth order, $\nu = 0.5$; - - ◇ - -, third-order high bandwidth, $\nu = 0.5$; ————, standard sixth order, $\nu = 0.1$; and - - - - -, third-order high bandwidth, $\nu = 0.1$.

still exists. The optimized preferred ENO operator, in which β_0 was restricted to $2\pi/7$, also has similar deviations; however, they are about 4% that of Tam-2 and are not visible on this scale. Figure 6c, which shows the absolute value of the wave number error, indicates clearly that the optimized preferred ENO operator is better than the Tam-2 operator, except in the narrow region S $(0.93 < \beta < 1.14$ or $5.5 < $ PPW $< 6.7)$.

The Fourier analysis presented in Fig. 6 describes how the methods perform at each time step. The metric developed earlier in Eqs. (2) and (3) builds on the Fourier analysis to predict the regime (the range of PPW or β) that is important to achieve a specific criterion on the accumulated error. Figure 7 shows the result of this metric for the preferred ENO operators and the Tam-2 operator. For the two preferred ENO operators, we have shown only the prediction based on the more restrictive amplitude criterion. In generating this result, the time step was set small so that the influence of the spatial operator could be isolated. The Tam-2 operator requires fewer PPW only if the propagation distance is relatively short. The jump that occurs at about 15 wavelengths is a consequence of the large error that was observed in that operator in Fig. 6c (at $\beta \approx 0.8$). The high-bandwidth preferred ENO operator provides an improvement of only 2–3 PPW over the standard preferred ENO operator. This can, however, result in a significant savings in realistic multidimensional problems where the criterion must be applied to the smallest wavelength of interest.

Note that the error in the preferred ENO operators is dominated by the imaginary part, which controls the dissipation. We feel this is an advantage in spite of the fact that many other researchers take great pains to design operators that are nondissipative. All discrete approximation operators have errors in either phase or amplitude; both will lead to incorrect results. Although amplitude errors are usually readily detectable, phase errors are usually less obvious. Yet in a nonlinear process, the phase relation of different modes can greatly influence their interaction. Thus not only should all modes that are important to a particular problem be resolved, but those that are not resolved should be either dissipated or filtered out. The slight upwind bias of the preferred ENO operator provides this needed dissipation.

Numerical Comparisons

The intent in designing high-bandwidth operators is to enable accurate calculations to be performed with fewer grid points. However, we first illustrate that the optimized operators are convergent and well behaved through a grid-refinement study. Figure 8 presents results obtained by a modified version of the ENO code applied to a linear advection problem in which a wave with an amplitude of 0.1 has propagated 10 wavelengths. For this case only, the stencil adaptation algorithm of the ENO code was disabled so that the preferred stencil was applied at every point. At moderately large CFL numbers ($\nu = 0.5$), the error of the third-order time integration used by the ENO code dominates the total error, and little difference is found between the standard operator and the high-bandwidth operator. When the CFL number is reduced ($\nu = 0.1$), the high-bandwidth operator is more accurate between 4 and 12 PPW, as expected. Both methods converge uniformly on the finer grids at the expected rate, and the standard sixth-order method is the most accurate on sufficiently fine grids. To provide perspective, at 8 PPW the high-bandwidth operator
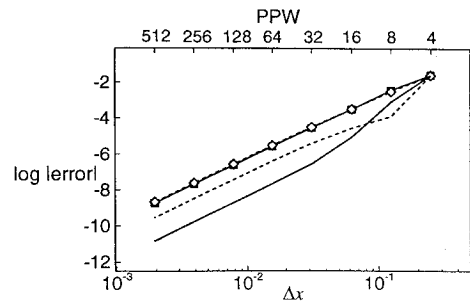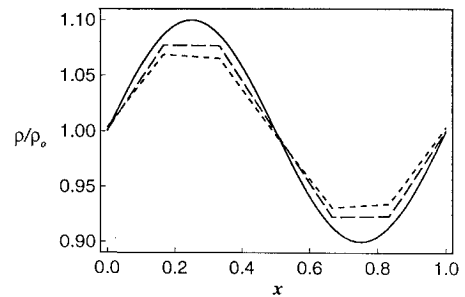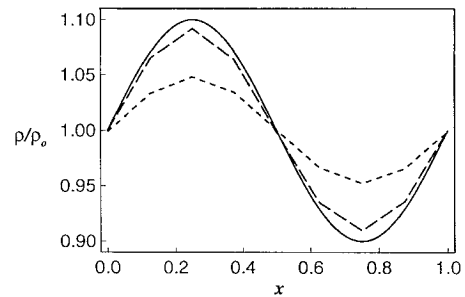

Fig. 9   Convection of a density perturbation: ————, analytic solution; - - - - -, sixth-order standard ENO; and — — —, third-order high-bandwidth ENO; a) 10 fundamental wavelengths propagation with six PPW and b) 100 fundamental wavelengths propagation with eight PPW.

has the same error as the second-order operator (used earlier in the paper) at 128 PPW.

In the numerical comparisons to follow, results labeled "standard sixth order" are produced by the original ENO code, and results labeled "third-order high bandwidth" are produced by replacing all standard sixth-order operators required by the ENO code with the optimized high-bandwidth operators. The stencil-adaptation algorithm within the ENO code has been enabled, and a CFL of $\nu = 0.1$ is used to highlight the difference between the two methods. However, such a low CFL number may not be necessary to take advantage of the high-bandwidth operator's improved performance.

When the Euler equations are solved for a periodic domain in which the initial profile includes a density perturbation in a uniform velocity and pressure field, the density perturbation advects at the speed of the ambient velocity without distortion. This Euler analogy to the linear advection equation is useful for illustrating improvements that can be gained by using the high-bandwidth operators we have described. In the following one-dimensional result, the initial density distribution is sinusoidal $[\rho/\rho_0 = 1. + 0.1 \sin(2\pi x)]$, and the velocity is set such that the freestream Mach number is 1.

In Fig. 9a, the results from the standard sixth-order and the third-order high-bandwidth version of the ENO code are shown. These results are obtained with 6 PPW, which the PPW analysis predicts to be adequate for the high-bandwidth operator. After 10 wavelengths
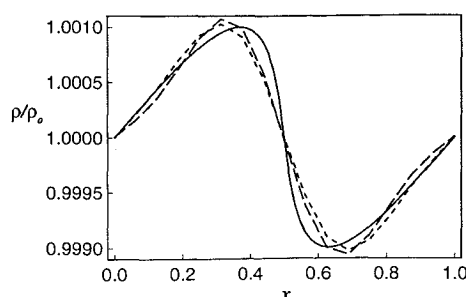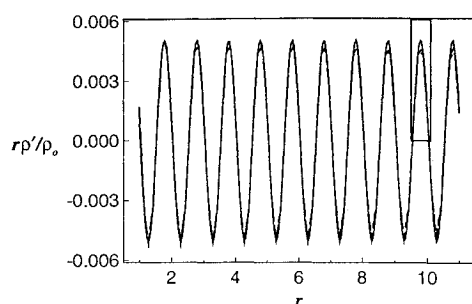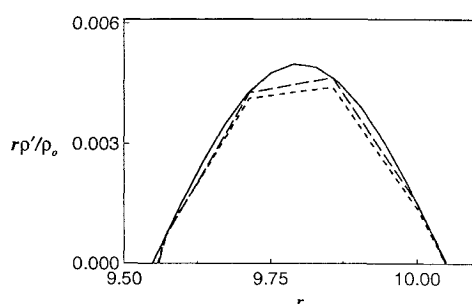
Fig. 10 Acoustic wave that has steepened after propagating 100 fundamental wavelengths: ———, Whitham's solution; - - - - -, sixth-order standard ENO; and — — —, third-order high-bandwidth ENO.

a)

b)

Fig. 11 Density fluctuation along axis of motion of a sphere oscillating at an oscillation Mach number M = 0.005 and frequency ω = 2π: —, analytic solution; - - - - -, sixth-order standard ENO; and — — —, third-order high-bandwidth ENO.

of propagation, the high-bandwidth results have less than a 10% error. Although the sixth-order results do not meet the criterion, the difference between the two sets of results is small, and an increase in resolution of only 1 PPW increases the accuracy of the standard scheme to meet this criterion. This result indicates that the third-order high-bandwidth scheme is only slightly better for short propagation distances. As the waves are allowed to propagate further, the difference becomes more apparent, as seen in Fig. 9b. In this case, the wave has traveled 100 wavelengths with 8 PPW. This resolution was chosen on the basis of the PPW analysis for the high-bandwidth operator. The third-order high-bandwidth solution closely resembles the exact answer, but the result from the standard sixth-order solution is highly dissipated.

One area in which the high-bandwidth scheme has an advantage over the standard scheme is in the resolution of harmonics. Because the number of points needed to resolve the mth harmonic must be multiplied by m to get the number of points required in the fundamental, any savings in a harmonic representation is multiplicative. Figure 10 presents results for the plane-wave problem, for which wave steepening is significant, but the wave has not yet shocked. This calculation is different from the previous plane-wave computation in that the waves are part of an infinite wave train that is solved on a periodic domain. Rather than being driven by a moving piston, here the flow is defined in terms of the initial nondimensional velocity profile $u(x) = M \sin(\omega x)$. To achieve a long

propagation distance without shocking, the selected amplitude of the velocity perturbation is small. In Fig. 10, results are shown for a wave with an amplitude $M = 0.001$ in which the fundamental mode has traveled 100 wavelengths with 16 PPW. Hence, the first harmonic has traveled 200 wavelengths with only 8 PPW. Even though only a small portion of the total energy is in the first harmonic, the third-order high-bandwidth result is slightly steeper. The higher harmonics, which become increasingly important as the wave begins to shock, are damped by both operators. When the waves shock, the difference between the standard sixth-order and the third-order high-bandwidth calculation is negligible.

The benefit of using the high-bandwidth operators carries over to two- and three-dimensional problems. Figure 11 shows results obtained for a two-dimensional oscillating sphere (the plotting of the solution is piecewise linear in the figure). For this calculation, a sphere is oscillated at a low Mach number so that a linear solution can be used for comparison purposes. The grid resolution of 7 PPW was chosen on the basis of the Fourier PPW analysis such that the standard sixth-order operator should be within 10% of the analytic solution. Although a slight decay is noticeable in the results for the standard sixth-order scheme, Fig. 11b, the error is within the 10% tolerance limit, and the results for the third-order high-bandwidth scheme are essentially the same as the analytic solution.

Conclusions

We have demonstrated that computational fluid dynamics methodology is applicable to acoustic problems; however, traditional low-order methods require excessively fine grids. High-order and high-bandwidth algorithms can provide the highly accurate calculations necessary in computational aeroacoustics. A PPW analysis that accounts for accumulated error in a propagating wave provides a means of estimating the resolution requirements of acoustic problems. The PPW analysis is also useful as a basis upon which to compare algorithms and can serve as a guide for improving algorithms. Standard high-order operators, such as the sixth-order operators found in the ENO code used here, are quite accurate, and significant performance improvement is difficult. The high-bandwidth approach does perform better primarily when the propagation distances are long relative to the wavelength; however, extreme care must be exercised in the design of high-bandwidth operators to prevent the introduction of significant error into the longer wavelengths. The high-bandwidth operators developed here had little influence on the resolution of captured shocks and were convergent and well behaved; they imposed no additional cost on the original ENO code while providing improved long-distance propagation characteristics.

References

[1]Thomas, J. P., and Roe, P. L., "Development of Non-Dissipative Numerical Schemes for Computational Aeroacoustics," AIAA Paper 93-3382, 1993.

[2]Lele, S. K., "Compact Finite Difference Schemes with Spectral-Like Resolution," Center for Turbulence Research Manuscript 107, NASA Ames Research Center/Stanford University, 1990.

[3]Tam, C. K. W., Webb, J. C., and Dong, Z., "A Study of the Short Wave Components in Computational Aeroacoustics," *Journal of Computational Acoustics*, Vol. 1, No. 1, 1993, pp. 1–30.

[4]Lockard, D. P., "An Investigation of Accuracy Requirements for Computational Aeroacoustics," M.S. Thesis, George Washington Univ., JIAFS, Hampton, VA, July 1993.

[5]Tam, C. K. W., and Shen, H., "Direct Computation of Nonlinear Acoustic Pulses Using High-Order Finite Difference Schemes," AIAA Paper 93-4325, 1993.

[6]Whitham, G. B., *Linear and Nonlinear Waves*, Wiley, New York, 1974, pp. 42–46 and 177–181.

[7]Jameson, A., Schmidt, W., and Turkel, E., "Numerical Solution of the Euler Equations by Finite Volume Methods Using Runge-Kutta Time-Stepping Schemes," AIAA Paper 81-1259, 1981.

[8]Atkins, H. L., "High-Order ENO Methods for the Unsteady Compressible Navier-Stokes Equations," AIAA Paper 91-1557, 1991.

[9]Shu, C. W., "Total-Variation-Diminishing Time Discretizations," *SIAM Journal of Scientific and Statistical Computing*, Vol. 9 No. 6, 1988, pp. 1073–1084.

[10]Tam, C. K. W., and Webb, J. C., "Dispersion-Relation-Preserving Finite Difference Schemes for Computational Aeroacoustics," *Journal of Computational Physics*, Vol. 107, 1993, pp. 262–281.